

Dendritic Growth Tip Velocities and Radii of Curvature in Microgravity

M.B. KOSS, J.C. LaCOMBE, L.A. TENNENHOUSE, M.E. GLICKSMAN, and E.A. WINSA

Dendritic growth is the common mode of solidification encountered when metals and alloys freeze under low thermal gradients. The growth of dendrites in pure melts depends on the transport of latent heat from the moving crystal–melt interface and the influence of weaker effects like the interfacial energy. Experimental data for critical tests of dendritic growth theories remained limited because dendritic growth can be complicated by convection. The Isothermal Dendritic Growth Experiment (IDGE) was developed specifically to test dendritic growth theories by performing measurements with succinonitrile (SCN) in microgravity, thus eliminating buoyancy-induced convection. The first flight of the IDGE in 1994 operated for 9 days at a mean quasi-static acceleration of $0.7 \times 10^{-6} g_0$. The velocity and radius data show that at supercoolings above approximately 0.4 K, dendritic growth in SCN under microgravity conditions is diffusion limited. By contrast, under terrestrial conditions, dendritic growth of SCN is dominated by convection for supercoolings below 1.7 K. The theoretical and experimental Peclet numbers exhibit modest disagreement, indicating that transport theories of dendritic solidification require some modification. Finally, the kinetic selection rule for dendritic growth, $VR^2 = \text{constant}$, where V is the velocity of the tip and R is the radius of curvature at the tip, appears to be independent of the gravity environment, with a slight dependence on the supercooling.

I. INTRODUCTION

DENDRITES are ramified, treelike crystals formed from a solidifying melt, occurring in many pure materials and alloy systems. Dendritic growth also provides an archetypal problem in morphogenesis, where a complex pattern evolves from simple starting conditions. As one of the simplest nontrivial examples of spontaneous pattern formation, the physical understanding and mathematical description of dendrites remains of interest to mathematicians, scientists, and engineers.

The growth of dendrites is known to be controlled by the transport of latent heat (and for alloys, solute) from the moving crystal–melt interface into the supercooled (super-saturated) melt. The transport of heat and solute combine with the interplay of weaker effects like surface tension, interface attachment kinetics, and ambient noise. Gradients of the melt's density near the solid–liquid interface, caused by the release of solute or latent heat, are acted upon by gravity. The gravitational body force results in buoyancy-induced melt flows affecting the overall transport conditions. Gravity-induced convection complicates how dendrites grow.

A series of microgravity experiments in dendritic solidification, the IDGE, first flew in low-Earth orbit aboard the space shuttle Columbia (STS-62) in March 1994, and again in February 1996 and November 1997. The experiments involved growing thermal dendrites in a pure material at precisely measured supercoolings, and photographing them

as they solidified. The local quasi-static acceleration field that promotes convection may be reduced on orbit to about one-millionth of its terrestrial value. The scientific objective of the experiments was to produce data sets of dendritic tip velocities and radii as benchmarks for critically testing theories of diffusion-limited dendritic growth. This article presents the final results and conclusions reached mainly from the first flight experiment. These experiments reveal for the first time large differences between dendritic growth occurring under terrestrial and microgravity conditions, as well as some disparities between the microgravity experiments and predictions based on theory.

II. BACKGROUND ON DENDRITIC GROWTH

The quantitative study of dendrites began with the heat-transport analysis of Ivantsov in 1947.^[1] Ivantsov's analysis only incorporates the conduction of latent heat from a dendrite, assumed to be paraboloidal and branchless. Over the past 50 years, a number of theories of steady-state dendritic crystal growth have been proposed (references within Glicksman and Marsh's review^[2]) that incorporate additional phenomena along with those in Ivantsov's formulation. In addition, numerical simulations of both time-dependent and steady-state dendritic growth have been investigated that combine heat transfer with certain interfacial conditions.^[3–6] For an exposition of key theoretical features of dendritic growth, see the introduction in Kunka, *et al.*'s recent article.^[7] Despite the multitude of more recent and sophisticated models, the Ivantsov model, when compared with an appropriate data set, provides critical insight into dendritic phenomena, and thereby more clearly identifies phenomena that need to be incorporated into predictive models of dendritic growth. Therefore, the Ivantsov model provides an excellent probe to examine the extent to which thermal diffusion limits dendritic growth and helps expose weaker physical effects

M.B. KOSS, Research Assistant Professor, J.C. LaCOMBE, Postdoctoral Research Associate, L.A. TENNENHOUSE, Graduate Research Assistant, and M.E. GLICKSMAN, John Tod Horton Professor, are with the Materials Science and Engineering Department, Rensselaer Polytechnic Institute, Troy, NY 12180-3590. E.A. WINSA, Project Manager, is with the Fluids and Combustion Facility, Microgravity Science Division, NASA-Glenn Research Center at Lewis Field, Cleveland, OH 44135.

Manuscript submitted June 23, 1998.

that, when combined with the transport of latent heat, result in dendritic pattern formation.

Ivantsov based his transport analysis on a suggestion made by Papapetrou,^[8] who, in 1935, first described the form of a dendritic crystal as a paraboloid of revolution with a fixed radius of curvature R , growing at a constant velocity V . Ivantsov's solution is as follows:

$$\Delta = Pe^P E_1(P) \equiv I_v(P) \quad [1]$$

This yields the dimensionless supercooling, $\Delta = (T_m - T_\infty)/(\Delta h_f/c_p)$, in terms of the Peclet number, $P = VR/(2\alpha)$, where Δh_f is the molar latent heat, c_p is the constant pressure molar specific heat, α is the thermal diffusivity of the melt phase, and $E_1(P)$ is the first exponential integral function. This also defines $I_v(P)$ as the Ivantsov function. Inasmuch as the supercooling, Δ , is in practice the independent variable, a more useful transport relation is the following:

$$P \equiv I_v^{-1}(\Delta) \equiv \frac{VR}{2\alpha} \quad [2]$$

where $I_v^{-1}(\Delta)$ is the formal inverse to Eq. [1]. Thorough discussions of solutions to the heat-diffusion equation for dendrites are available in Langer's review^[9] and Pelce's book.^[10]

It is well known that the transport solution alone, Eq. [1], provides an incomplete description of steady-state dendritic growth insofar as it specifies only the Peclet number. The observable experimental variables V and R are not independently predicted. Ivantsov's description of the process is underdetermined, as it provides one equation for the two unknowns.

Since the mid-1970s, efforts within the physics community have been directed to answering the question as to whether, and under what conditions, a second independent equation exists that, when combined with the Ivantsov diffusion solution, "selects" the dendritic operating state. Langer and Muller-Krumbhaar^[11] suggested that dendrites grow at the margin of stability and that the steady-state tip radius is related to the thermal diffusion length, α/V , and the capillary length, d_0 , which can be calculated from the following:

$$d_0 = \frac{\Omega \gamma \left(\frac{c_p}{\Delta h_f} \right)}{\Delta s_f} = \frac{\Omega \gamma c_p T_m}{\Delta h_f^2} \quad [3]$$

where Ω is the molar volume, Δs_f is the molar entropy of fusion ($\Delta h_f/T_m$), and γ is the solid-liquid interfacial energy. This yields the following necessary second equation:

$$\sigma^* \equiv \frac{2\alpha d_0}{VR^2} \approx \frac{1}{4\pi^2} \quad [4]$$

where σ^* is a scaling or selection constant. In the years since this initial work, Langer, Levine, and others (references in Langer^[12] and in Brenner and Mel'nikov^[13]) corrected and adapted these ideas in the development of steady-state theories that specify that surface-energy anisotropy is key in selecting a unique dendritic operating state. Similar scaling equations can also arise from different dynamical considerations (references in Glicksman and Marsh^[2]), but with the results almost always expressible through a scaling constant, as shown in Eq. [4]. Thus, solving Eqs. [2] and [4] for V and R yields the following:

$$V = \frac{2\alpha\sigma^* I_v^{-2}(\Delta)}{d_0} \quad [5]$$

and,

$$R = \frac{d_0}{\sigma^* I_v^{-1}(\Delta)} \quad [6]$$

where V and R are now unique observables of steady-state dendritic growth, depending only on the supercooling and material constants.

A great deal of the more recent experimental work concerning dendritic growth has been performed using succinonitrile (SCN) since Glicksman *et al.*^[14] first grew and photographed SCN dendrites in the early 1970s. SCN [NC(CH₂)₂CN], an organic plastic, is an excellent experimental system for studying dendritic growth as it solidifies similarly to the cubic metals; *i.e.*, with a molecularly "rough" solid-liquid interface, but also has a convenient melting temperature (~ 58.08 °C), excellent chemical stability, and optical transparency. In addition, there now exist accurately known thermophysical properties for SCN. Thus, SCN facilitates *in situ* dendritic growth studies, permitting dendritic tip velocities and radii to be measured accurately and then used to test theories.

The SCN (99.99 pct pure or better) data of Glicksman *et al.*^[14] were consistent with a scaling constant of $\sigma^* \approx 0.019$, which was in reasonable agreement with the theoretical value 0.025. However, this particular experimental σ^* value was obtained over a limited supercooling range, with uncertainties in the observed tip radii that were too large to allow definitive conclusions. Huang and Glicksman^[15] later performed more refined experiments on high-purity SCN (better than 99.999 pct pure) at smaller supercoolings where the velocities are slower and the tip radii are larger, permitting more precise measurements. In this work, however, Huang and Glicksman showed that gravity-induced convection can *dominate* the heat transport during dendritic growth, especially in the lower supercooling range of their experiments.^[16]

In order to deal with the enhancement of heat transfer from gravity-driven convection, there have been a number of studies modeling the influence of natural or forced convection on dendritic growth; *e.g.*, Saville and Beaghton,^[17] Ananth and Gill,^[18,19] and more recently Sekerka *et al.*^[20] These hydrodynamic models include gravitational effects, but these effects are frequently coupled back to as yet unproven elements of basic dendritic growth theory, and consequently have not provided an independent test of the theory.

Experiments performed at higher supercoolings, where convective influences diminish in comparison to thermal conduction, did not clarify the situation either. The morphological scale of dendrites becomes too small to be resolved at the high growth speeds encountered. Thus, the experimental situation prior to the microgravity experiment reported here was that there was too narrow a range of supercoolings in any dendritic system studied terrestrially that remained tolerably free of convection effects and simultaneously permitted accurate determination of the dendritic tip radius. This necessitated a microgravity dendritic growth experiment to measure definitively the kinetics and morphology of convection-free dendrites in SCN.^[21,22]

III. THE ISOTHERMAL DENDRITIC GROWTH EXPERIMENT

Designated the IDGE, the first flight, manifested on the United States Microgravity Payload-2 (USMP-2) mission, was launched and operated on the Space Transportation System-62 (STS-62) on March 4 through 14, 1994. Three of the authors of this article have published elsewhere an article detailing the criteria and chronology of preparing for this flight experiment.^[23] The IDGE enabled the acquisition of accurate dendritic growth speed and morphology data under well-defined heat-transfer conditions by greatly reducing buoyancy-induced convective heat transport through the near-elimination of gravity.^[24] As shown in this article, the microgravity environment expands the range of super-coolings useful for testing diffusion-based theories of dendritic growth and permits an assessment of both transport theory and the interfacial physics of the selection/scaling rule.

A. IDGE Apparatus

The experimental techniques for accomplishing simultaneous kinetic and morphological measurements for SCN dendrites are now well established.^[14,15] However, the constraints of an autonomous, or tele-operated, microgravity experiment required extensive modification of established ground-based laboratory techniques.^[21,25,26] This became most evident in the design and construction of the flight growth chamber (Figure 1), which is of central importance to the operation of the IDGE space flight instrument.

In order to withstand the launch accelerations and the other rigors and safety requirements associated with space flight, the typical delicate laboratory growth chamber used in prior studies of dendritic growth was replaced by a space-qualified design constructed solely of 300-series weldable stainless steel with borosilicate glass windows. The flight chamber provides two perpendicular unobstructed views of the growing dendrites through four optically polished windows. This allows stereographic corrections to the velocity and radius of curvature measurements. This type of chamber requires that the dendrites grow within a restricted field of view defined by the optics. This requirement was met by providing a thin injector tube, called the "stinger," that locates the precise point within the growth chamber where unconstrained dendritic growth starts. Dendritic growth itself

is initiated by energizing a thermoelectric cooler attached to the end of the stinger that is external to the central volume of the growth chamber. The other end of the stinger, the aperture, where dendrites emerge into the central volume of the chamber, is shaped like the tip of a fountain pen. This design helps produce, and eventually isolates, a single leading dendrite, thereby reducing the time needed for the dendrite tip to achieve steady-state conditions.

A compliant stainless-steel bellows accommodates the volume change of the melt as it warms, cools, or changes phase. The growth chamber, with its charge of ultrapure (99.999 pct) SCN, is sealed hermetically under vacuum. During the experiment, the external pressure (approximately 2 ± 0.1 bar), continuously transmitted through the bellows from the surrounding thermostatic bath, is maintained by actuators to be sufficiently constant to prevent either free surface formation due to cavitation in microgravity, or buildup of significant pressure gradients across the optical windows. The joining of all stainless-steel chamber components, and sealing of its orifices in the areas that contact the SCN, is performed with autogenous electron beam welds. This joining and sealing method protects the high purity of the SCN test material from contamination by avoiding the introduction of any solder, fluxes, elastomers, or other substances that might, over time, contaminate the SCN during the long stowage period preceding the launch.^[26]

The growth chamber is mounted inside a temperature-controlled pressurized tank or thermostat (Figure 1). The thermostat is filled with a mixture of ethylene glycol and water mixed in a proportion such that its index of refraction matches that of molten SCN. Index matching of the heat-transfer fluid enhances the performance of the IDGE optical system. Two heaters and a mixing propeller at the base of the thermostatic tank permit temperature control to the desired level (within ± 2 mK of set point) both temporally and spatially. Temperatures are monitored at various locations both inside the thermostat and within the growth chamber to ± 0.001 K.

Photographs are the primary data for both tip-velocity and tip-radius measurements. The IDGE employs a modified shadowgraphic system to obtain sufficiently high-resolution photographic information of growing dendrites with a *fixed focus* lens system. A collimated blue light beam back lights the growing dendrites. The source of this light is an incoherent broadband xenon flash that is transmitted through a diffuser, a 1-mm pinhole aperture, a collimating lens, and a 486-nm NBP filter. The dendrite is imaged during growth with a 1.8-mm "cleaning aperture," and a series of relay lenses that transmit the shadow image, at a magnification of approximately 1.87 times, to the film plane. The magnification represents a compromise between the large field of view required and adequate optical resolution for the super-cooling range. The optic system records light that remains collimated as it goes through the optic system. The light that strikes the curved solid dendritic interface that has a different index of refraction from the surrounding molten SCN is refracted and no longer collimated. The noncollimated light rays are blocked by the cleaning aperture and a shadow of known magnification is created and recorded on film. A second optical path, partially superimposed on the first using dichroic mirrors, is back lit by a red LED and projected onto an optical RAM camera. This is used for

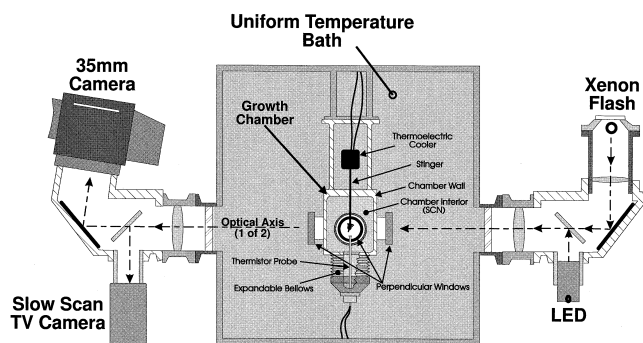


Fig. 1—Schematic of the IDGE stainless steel growth chamber, thermostatic bath, and optic system. Both perpendicular paths through the windows of the growth chamber (only one shown in the figure) contain both the film and electronic image optical paths.

electronic detection of dendritic growth, and to provide near-real-time digital telemetry.

The growth chamber, photographic-optic system, control electronics, and power and temperature distribution system are attached to a support rack that is housed within the experiment apparatus container (EAC), which is a barrel-like double-walled structure protected from both excessive heat loss and solar heating by a multilayer thermal insulation blanket. The inner pressurized vessel of the EAC contains an atmosphere of moist nitrogen at 1 bar, maintained at 25 ± 2 °C. The 310-kg 1-m-long flight instrument is mounted on the support structure in the orbiter bay of the USMP carrier. The carrier provides the IDGE with power, freon, communication, and a ± 0.01 -second resolution IRIG-B Greenwich Mean Time (GMT) timing signal. The carrier is mechanically and electrically connected with the payload bay of the space shuttle Columbia. Two accelerometers from the tri-axial space acceleration measurement system (SAMS) provide $10\text{-}\mu g_0$ resolution (0.01 to 5 Hz) and are mounted inside the IDGE's EAC and on the carrier. A tri-axial quasi-static accelerometer from the orbital acceleration research experiment (OARE) provide $0.1\text{-}\mu g_0$ resolution near 0 Hz, and is mounted on the shuttle keel.

B. Experiment Procedures

The purity of the SCN test material was confirmed by examining in orbit the flatness and duration of the temperature-time melting plateau. The liquidus temperature of the SCN was measured by locating the peak recalescence temperature when the supercooled melt solidifies at a supercooling of 1 K. The peak recalescence temperature established the calibration datum from which all subsequent supercoolings were measured. The bulk of the experiment duration was comprised of individual dendritic growth cycles where dendrites are grown and photographed at selected supercoolings.

Prior to initiating each dendritic growth cycle, the thermostatic bath is heated in excess of 3 K above the SCN ambient pressure melting temperature (~ 58.12 °C). The bath is maintained at this temperature until the SCN inside the chamber completely melts and achieves uniform temperature. The bath temperature is then reduced to produce the desired level of supercooling in the SCN. After the molten SCN has uniformly supercooled (approximately 1 hour), the thermoelectric coolers are energized to nucleate the solidification at the capped end of the stinger. The solidifying SCN grows down the inside wall of the hollow stinger, until it emerges from the stinger aperture as a freely growing dendritic crystal located near the center of the growth chamber.

Upon emerging from the stinger, the dendrite undergoes a short transient growth phase and then achieves a steady-state growth velocity, which is maintained until the thermal field of the dendrite interacts with the solidification along the walls, or the tip of the dendrite grows out of the field of view. The RAM camera system monitors the tip of the stinger, and when a crystal emerges, the photographic sequence is triggered (Figure 2). For each dendritic growth cycle, the experiment produces the following: a time series of stereo-pairs of 35-mm photographic images; bi-level (black and white) digital images from the RAM camera; acceleration spectra from the SAMS and OARE instruments;

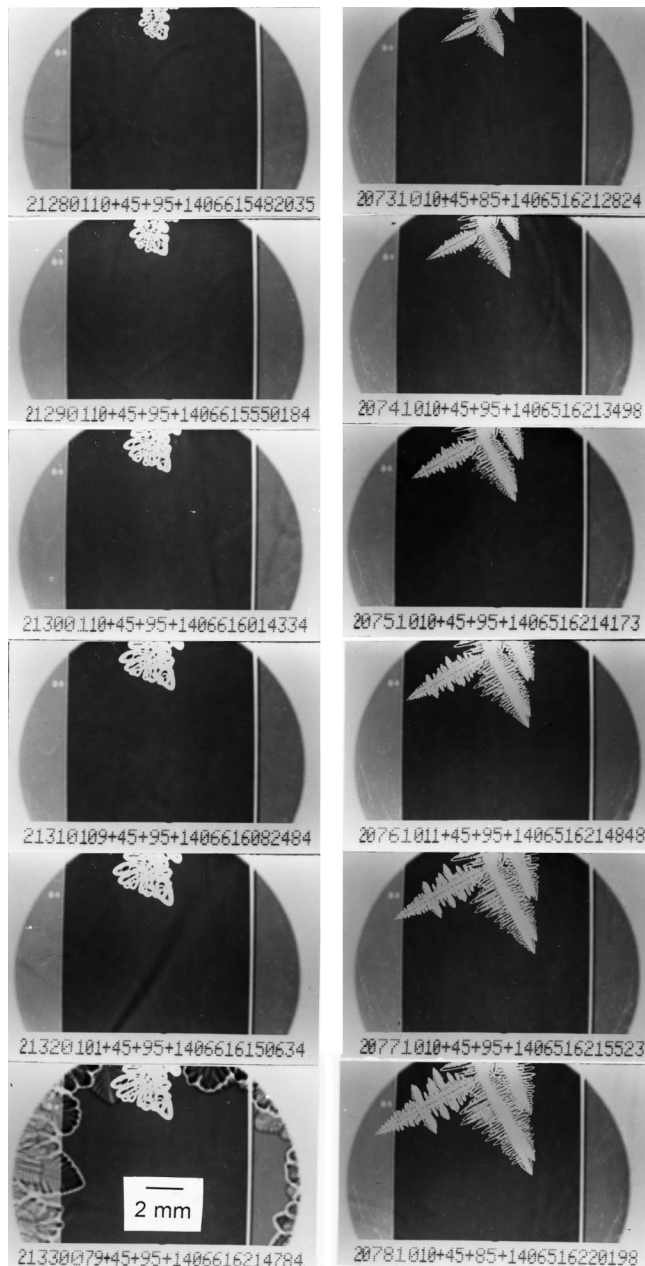


Fig. 2—Sample of two photonegative sequences from the flight experiment. The first sequence running down the page is at a supercooling of approximately 0.11 K with photographs taken every 6 min and 42.5 s. On the last photo, the solid is forming on the surface of the window. The second sequence is at a supercooling of approximately 1.02 K with photographs taken every 6.75 s.

and ancillary data streams characterizing the internal pressure and temperature of the growth chamber and thermostatic bath. All of these data, excepting the 35-mm film, are available *via* telemetry in near-real time. The photographs were naturally only available post-flight.

C. Data Reduction

Velocities are measured from the slopes of the dendrite tip displacement *vs* time curves. The first step in generating tip displacement curves is selecting the dendrite of interest

for each photonegative frame, and measuring its tip coordinates in both views as a function of time. These measurements were performed using a two-axis precision stage with digital readouts and a tri-ocular charge coupled device (CCD) camera system. The film frame is mounted and oriented on the stage, with an image taken by the CCD camera sent to a monitor. The X and Y positions of the solid–melt profile are recorded with reference to an arbitrary origin that locates the dendrite tip to a resolution of about $\pm 4 \mu\text{m}$ in the film plane. Locating the tip position is aided by using an oscilloscope that can display a single scanned TV line from the image, thus achieving a resolution of the dendrite tip position of approximately $\pm 2 \mu\text{m}$.

The slopes of the X , Y tip coordinate data observed along the two optic axes give the projected growth orientation angles for each corresponding view of the dendrite. The growth orientation angles are time independent along the entire growth path. Growth angles measured in this manner are accurate to better than ± 1 deg. These orientation angles are also related to the shuttle's orbital coordinate system for the purposes of correlating the calculated growth velocity measurements with the tri-axial OARE acceleration data. Finally, the growth-axis orientation angles are used to make the required stereographic corrections to calculate the dendrite's true growth speed. Thus, for each optical axis, a tip-displacement vs time curve (Figure 3) is formed and modified for film magnification and stereographic projection. The slope of the displacement vs time curve, which is the growth speed, is determined by performing several least-squares regressions to the displacement-time curve, using different ranges of the tip-displacement data to include only those data obtained during steady state. This is necessary, since during some growths the dendrite eventually began to interact with the solid growing along the growth chamber's wall (see frost pattern on the last photographic frame of the low supercooling growth in Figure 2), slowing down the dendrite (Figure 3). In no case, within the measurement accuracy, did we see evidence of a dendrite speeding up as it approached a cold wall. The best fit selected in this manner yields the growth velocity, along with an estimate of its uncertainty, which is usually better than ± 2 pct. The growth-speed data derived independently from each optic axis generally agree within the stated uncertainties. This procedure also identifies the duration over which the dendrite achieves steady-state growth. The supercoolings specified for each dendritic growth cycle are averages taken over this steady-state time.

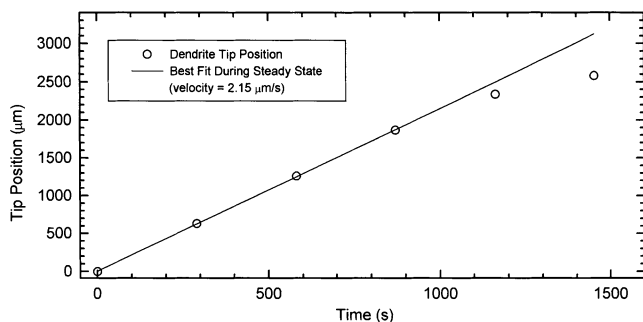


Fig. 3—Dendrite tip position-time plot at a supercooling of 0.141 K measured from a sequence of 35-mm photonegatives exposed during the flight experiment. The velocity taken from these data uses only the first four tip positions as the last two are no longer part of a steady-state growth.

The data for the tip-radius measurements reported here are obtained from the 35-mm photomicrograph negatives, each exposed during the steady state. The image analysis procedures used for extracting the steady-state shape of dendrite tips have been discussed in previous articles,^[27,28] but are summarized here for completeness. Once an image is selected from the camera that is in best focus, the negative is digitized using a microscope-mounted CCD camera connected to a PC-based image processing system. The hardware captured 256 levels of gray in an array of 480 lines by 512 pixels. The final result is an image resolved from 1 to 4 microns per pixel or line depending on the size of the field of view chosen for image capture.

Several image processing operations are performed. The image is corrected for nonuniformity in the lighting used to digitize the 35-mm film negative. Nonlinear effects introduced by the film-developing process are corrected from grayscale data obtained from a pair of neutral density filters that are imaged at the edges of every photograph. These filters reduce by a known ratio the incident light striking the film that formed the dendrite image. The image is then inverted to obtain a positive image that duplicates the light intensity profile at the dendrite.

Once the filtered image has been obtained, the position of the solid–melt interface is located. The solid–melt interface is assumed to be located at the pixel intensity representing 50 pct of the average background illumination. This is accomplished by locating the position of this intensity for each digitized line comprising the image. The coordinates of these points, recorded to subpixel resolution by an interpolation routine, define the solid–melt interface for that row of pixels. After repeating this for every row of pixels comprising the image, one has a set of coordinate pairs defining the dendrite's profile. These coordinates are then corrected for stereographic correction, film magnification, and image-capture magnification. This set of data is then used to calculate the radius of curvature at the tip. In Reference 27, two of the authors of this article have discussed some of the alternate ways of locating the crystal–melt interface as used by other researchers.

The measured data set of the dendrite tip is approximated by a smooth fourth-order polynomial of the following form:

$$y = y_0 + \frac{1}{2R}(x - x_0)^2 + q(x - x_0)^4 \quad [7]$$

where R represents the tip radius of curvature, and the coefficient q has units of length^{-3} , giving the amplitude of the leading-order deviation from a paraboloid of revolution. The magnitude and sign of q varies, depending on which direction the dendrite is viewed. In this procedure, the tip radius, R , is assumed, and appears to be constant when viewed from any direction. The set representing the profile of the dendrite is fit to Eq. [7] to produce the coefficients q and R (and x_0 and y_0). The results of a regression applied to this set are influenced by the fact that all the ordered pairs in the set representing the observed interface location are not of uniform quality. Close to the tip, for example, optical effects make finding the edge location difficult, whereas far from the tip, side-branching distortions become large enough to cause departures from the assumed smooth fourth-order shape.

To identify the best range of profile data to use in the

shape regression, the regression process is carried out with varying ranges of data. Initially, the range is taken from the tip to the first 50 pairs of interface points. Then the data range is extended to include the first 60 pairs of points, and so on. Each of these ranges incorporates all the profile data from the tip to the chosen cutoff. The values of the calculated radius of curvature should remain constant for a dendrite profile described exactly by the fourth-order polynomial in Eq. [7]. An examination of R as a function of the sample range from the tip (Figure 4) shows that the radius varies for data near the tip region, as is also the case when the sampling range extends too far from the tip into the side-branching region. Between these two limits, however, remains a sampling range over which the tip radius is essentially constant. The average radius of curvature and its associated standard deviation are obtained by applying this procedure in the intermediate sampling range. The uncertainty in the measured radii values is estimated primarily from the standard deviation values calculated during the regression and averaging process. The uncertainty of a radius measurement made from several frames, analyzed as described previously is determined from a combination of the R values and the associated uncertainties estimated from each photomicrograph. The tip radii of curvature reported here are accurate to within ± 5 pct for supercoolings less than 1.0 K.

IV. RESULTS AND DISCUSSION

Of the 57 dendritic cycles performed during the experiment, we recorded 37 steady-state velocities and radii over the supercooling range 1.011 to 0.064 K, and four steady-state velocities without accompanying radii measurements

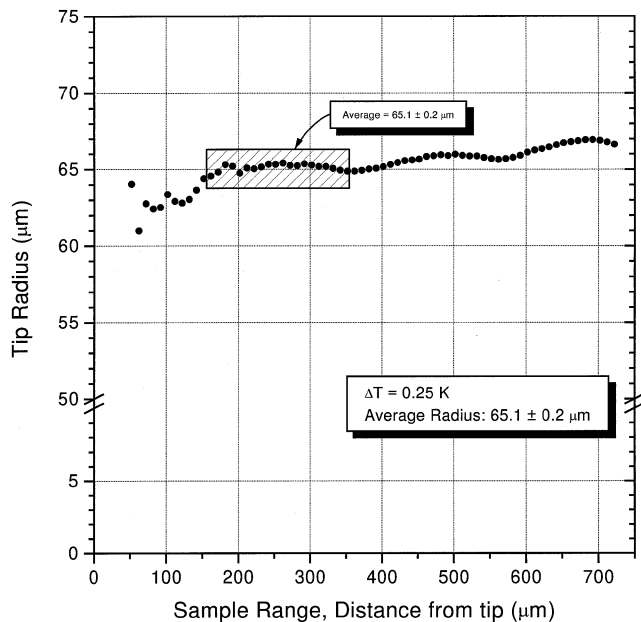


Fig. 4—Dendrite tip radius of curvature regressed from the dendrite's solid-liquid interface profile as a function of the sample range from the tip of the dendrite. For small sample ranges, the scatter in the position of the interface makes measurements imprecise, and at large sample ranges, the emerging side branches make measurements imprecise.

from 1.844 to 1.311 K supercooling (Table I). Prior to the microgravity flight experiment, the IDGE instrument was used for terrestrial dendritic growth cycles applying procedures identical to those in the flight experiment. In this manner, the instrument produced an additional 63 steady-state velocities and radii in the supercooling range 1.005 to 0.102 K, and three steady-state velocities from 1.306 to 1.104 K supercooling (Table II). In the discussion that follows, the microgravity and terrestrial data (Figures 5 and 6) are compared to terrestrial velocity and radii data reported in Huang and Glicksman^[15] over a comparable supercooling range, and the velocity data set of Glicksman *et al.*,^[14] over the supercooling range of 2.0 to 10 K (Figure 7). In addition, these data are used to calculate and compare values for the Peclet number, P , and the selection constant, σ^* (Figures 8 and 9).

Table I. Microgravity Dendritic Growth Velocity and Radius Calculations from 35-mm Photonegatives Exposed during Operations of the IDGE Apparatus on USMP-2/STS-62

$\Delta T \pm 0.002$ (K)	Velocity ($\mu\text{m/s}$)	Uncertainty ($\pm \mu\text{m/s}$)	Radius (μm)	Uncertainty ($\pm \mu\text{m}$)
1.844	923	18	—	—
1.753	756	15	—	—
1.573	571	4	—	—
1.311	343	1	—	—
1.011	169.8	0.5	14.3	0.8
1.010	171	3	14.5	0.2
0.783	85.3	0.3	19.7	0.4
0.782	87.6	0.2	18.7	0.3
0.781	87.2	0.3	19.8	0.3
0.612	46.2	0.1	26.7	0.7
0.612	46.34	0.05	25.9	0.5
0.473	23.28	0.05	35.9	0.2
0.471	24.55	0.07	34.8	0.8
0.413	20.8	0.2	38	2
0.373	14.17	0.04	44.9	0.5
0.371	14.44	0.07	46.2	0.3
0.291	8.4	0.2	58.1	0.3
0.290	8.45	0.04	58.5	0.5
0.262	6.58	0.03	66	1
0.233	5.42	0.02	73.2	0.4
0.232	4.6	0.1	77.5	0.1
0.231	5.0	0.2	71.7	0.5
0.229	5.5	0.2	70	2
0.183	3.60	0.07	89.2	0.6
0.182	3.1	0.2	91.3	0.3
0.182	3.43	0.02	90.6	0.2
0.182	3.33	0.02	93.0	0.4
0.181	3.16	0.03	95.1	0.7
0.181	2.82	0.02	93	4
0.152	2.41	0.01	108	1
0.142	2.04	0.01	116	1
0.142	2.00	0.01	113	4
0.141	2.15	0.01	114.6	0.8
0.112	1.2	0.1	155	15
0.111	1.21	0.01	133	14
0.111	1.27	0.01	141	4
0.103	1.16	0.01	154	2
0.092	1.03	0.02	157	7
0.089	0.95	0.01	155	10
0.088	0.91	0.07	158	4
0.064	0.53	0.01	218	35

Table II. Terrestrial Dendritic Growth Velocity and Radius Calculations from 35-mm Photonegatives Exposed during Operations of the IDGE Apparatus Prior to Its Use for the Microgravity Experiments on USMP-2/STS-62

$\Delta T \pm 0.002$ (K)	Velocity ($\mu\text{m/s}$)	Uncertainty ($\pm \mu\text{m/s}$)	Radius (μm)	Uncertainty ($\pm \mu\text{m}$)
1.306	390	5	—	—
1.104	275	2	—	—
1.104	275	3	—	—
1.005	220	4	11.6	0.5
1.005	229.0	0.4	12.4	0.2
1.002	220	3	12.9	0.9
1.002	223	5	14	1
0.776	133.7	0.6	17.4	0.4
0.775	130	2	16	2
0.773	135	3	16.2	0.5
0.773	129	3	16.1	0.6
0.607	75	2	21	2
0.606	79.7	0.1	20.2	0.4
0.605	82.7	0.8	19	1
0.603	80.5	0.9	19.8	0.6
0.465	49.5	0.6	23.7	0.3
0.465	51.8	0.2	23.9	0.3
0.463	49.6	0.7	23	2
0.463	50.6	0.2	24.3	0.5
0.462	48.8	0.5	21	1
0.366	31.5	0.8	30.0	0.7
0.363	31.8	0.2	30.9	0.2
0.363	31.4	0.1	30.7	0.7
0.285	20.5	0.2	37.8	0.4
0.285	20.8	0.3	36.5	0.1
0.285	20.6	0.1	37.5	0.6
0.284	20.44	0.06	36.7	0.6
0.283	19.6	0.2	37	1
0.282	19.8	0.1	38	1
0.226	13.88	0.04	43.6	0.6
0.225	14.0	0.1	43.4	0.1
0.225	13.8	0.1	49	1
0.224	12.4	0.1	45.4	0.5
0.224	12.7	0.1	47.5	0.7
0.223	13.38	0.08	45.8	0.3
0.223	13.18	0.08	46.4	0.4
0.223	13.3	0.1	46.3	0.7
0.222	13.34	0.06	46.5	0.2
0.222	13.0	0.2	47.1	0.3
0.222	13.1	0.2	46.9	0.4
0.175	8.96	0.04	55	1
0.175	8.5	0.1	55.6	0.2
0.175	8.78	0.05	54.8	0.1
0.174	8.6	0.1	57.7	0.5
0.174	8.4	0.1	58	1
0.173	8.6	0.1	58.2	0.2
0.173	8.35	0.08	58.5	0.3
0.173	8.4	0.1	58	1
0.172	8.3	0.2	59	1
0.172	8.43	0.05	59.5	0.9
0.172	8.3	0.3	58.8	0.7
0.136	5.72	0.02	73	2
0.135	5.62	0.02	69.3	0.2
0.135	5.62	0.01	72	2
0.134	5.16	0.06	73.4	0.5
0.134	5.41	0.04	73	2
0.133	5.40	0.03	72.2	0.4
0.133	5.33	0.08	73.6	0.3
0.133	5.30	0.05	73.6	0.5

Table II. Continued

$\Delta T \pm 0.002$ (K)	Velocity ($\mu\text{m/s}$)	Uncertainty ($\pm \mu\text{m/s}$)	Radius (μm)	Uncertainty ($\pm \mu\text{m}$)
0.132	5.3	0.1	72.1	0.6
0.132	5.39	0.04	73	2
0.106	3.74	0.04	87	2
0.105	3.72	0.05	90.3	0.7
0.105	3.74	0.01	84	1
0.102	3.35	0.06	94	1
0.102	3.41	0.06	94	2

A. Velocity Data

The two overlapping independent terrestrial dendritic growth velocity data sets (Glicksman/Huang and the terrestrial IDGE) used here for comparison with the new microgravity data are in good agreement with each other over the entire supercooling range (Figure 5). Only minor differences exist, arising most probably from the different angle of the [100] dendrite growth direction with respect to gravity (between 0 and 45 deg). Striking differences appear between the terrestrial growth velocity data and those obtained under microgravity conditions, particularly at the lower supercoolings. Even at supercoolings as high as 1.7 K, there still appears to be a small (approximately 10 pct) reduction in the growth velocity under microgravity conditions, as compared to terrestrial conditions. This reduction in velocity becomes even more evident at 1.3 K supercooling, where the velocity measured in microgravity is 15 pct lower than the terrestrial data. The difference between the two data sets increases to about 200 pct at small supercoolings. These results show that substantial convective effects are present at $1g_0$, even up to the highest supercoolings for which the solidification microstructures have been resolved to date.

In an earlier publication of the IDGE space flight results, using the *in situ* digital RAM camera data only,^[24] we showed that the velocity data could be consistently correlated with diffusion theory combined with a self-consistent velocity scaling constant, σ_v . This adjustable parameter was obtained by least-squares fitting the microgravity velocity data, and finding the value for σ_v , from the scaling expression for σ^* in Eq. [6], as follows:

$$\sigma_v = \frac{d_0 V_{meas}}{2 \alpha I_v^{-2} (\Delta)} \quad [8]$$

By again treating the scaling parameter, σ_v , as adjustable, we are able to calculate a self-consistent σ_v for each measured velocity from the photonegatives. We were not able to find a unique value of σ_v for the entire range of microgravity velocity data observed with the IDGE. However, at supercoolings above 0.47 K, all the observed microgravity velocity data correlated with the value $\sigma_v = 0.0175 \pm 0.0001$. In other preliminary publications,^[23,29–32] a different value for σ_v was reported due to the use of slightly different values for the thermophysical properties of SCN. The issue of the use of thermophysical properties in dendritic growth models of SCN is discussed in the Appendix to this article.)

The agreement in this supercooling range between theory and the dendritic velocities observed in microgravity, using one adjustable parameter, provides a necessary but not sufficient condition for demonstrating the validity of the thermal

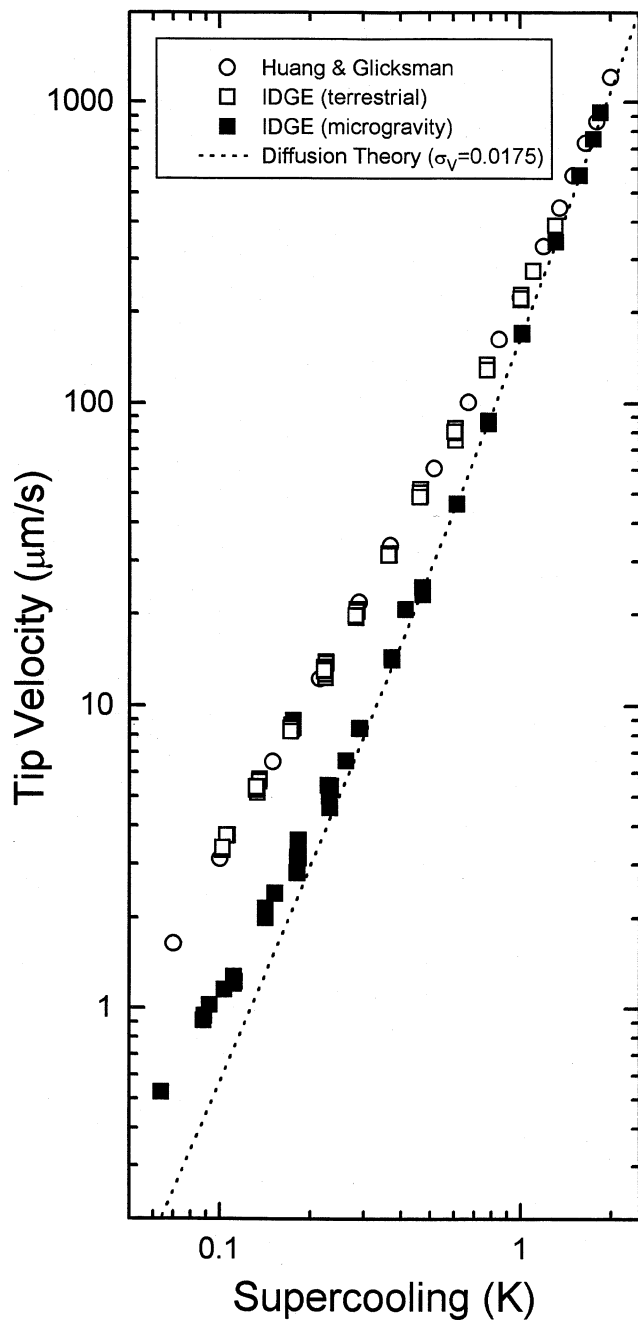


Fig. 5—Steady-state dendritic growth velocity vs supercooling. Dendritic growth velocities of succinonitrile observed in microgravity differ substantially from those measured under terrestrial conditions. The microgravity and terrestrial data sets converge at approximately 2.0 K supercooling. The data above 0.45 K supercooling can be fit to the combined Ivantsov–Scaling rule theories with a scaling constant of $\sigma_v = 0.0175$.

diffusion model combined with a *unique* scaling constant, σ^* . For compelling support of this theory, the radii data must also be correlated by the same σ^* value. However, we note that the agreement of theoretical velocity calculations with the microgravity data is limited to the range 0.47 to 1.85 K, thus indicating that this is the valid supercooling range over which one may test theories. In addition, when the σ_v generated from the microgravity-measured velocities in the supercooling range 0.47 to 1.85 K is used to predict

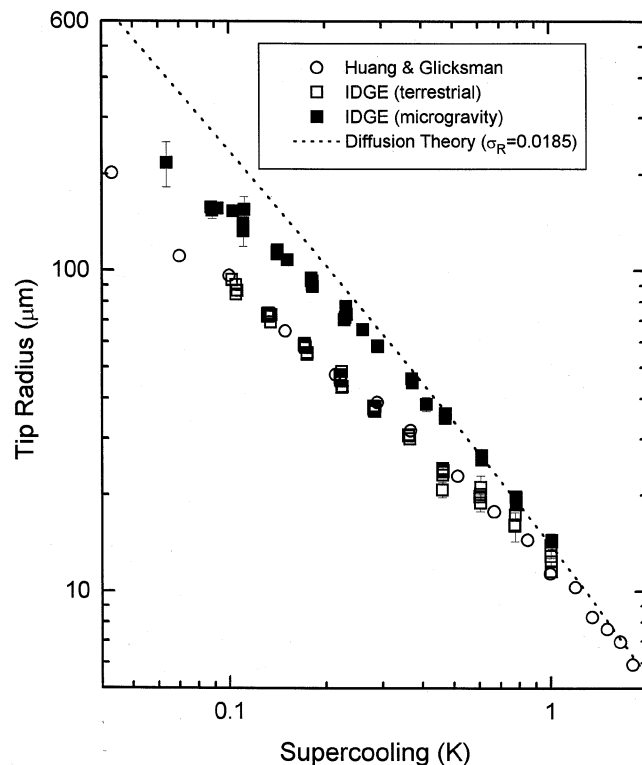


Fig. 6—Steady-state dendritic tip radius of curvature vs supercooling. Dendritic tip radii of succinonitrile observed in microgravity differ substantially from those measured under terrestrial conditions. The data above 0.45 K supercooling can be fit to the combined Ivantsov–selection theories with a scaling constant of $\sigma_R = 0.0185$.

velocities in the range 2.0 to 5.0 K (Figure 7), the predictions agree with the velocity data reported by Glicksman *et al.*^[14] Above a supercooling of about 5.0 K, the dendritic speeds become so high that interfacial kinetic effects may reduce the observed velocity below the diffusion-limited values calculated here using σ_v .

The slope of the observed microgravity velocity data (Figure 5) changes from being steeper than the observed terrestrial data at the higher supercoolings to almost parallel at supercoolings less than approximately 0.4 K. The deviations found between the velocity prediction using σ_v and the microgravity data obtained at the lower supercoolings suggest that: (1) a residual quasi-static microgravity level of only $0.7 \mu g_0$ has a significant effect on dendritic growth kinetics at small supercooling;^[20] or (2) the dendritic thermal field is interacting with the growth chamber walls.^[33] Thus, at sufficiently low supercoolings, an effect arises that substantially alters the growth velocity from what would be predicted from heat-conduction theory with the outer boundary conditions set at infinity. Last, we note that at the lower supercoolings, repeated velocity measurements taken at the same supercooling display significantly greater run-to-run differences than those at higher supercoolings where the scatter is barely discernible. The increased scatter in the growth speed might again be related to: (1) variations in the quasi-static acceleration levels during each growth cycle, combined with the random variation for each growth cycle in the angle between the dendrite axis and the residual microgravity vector; (2) the random direction that the growing

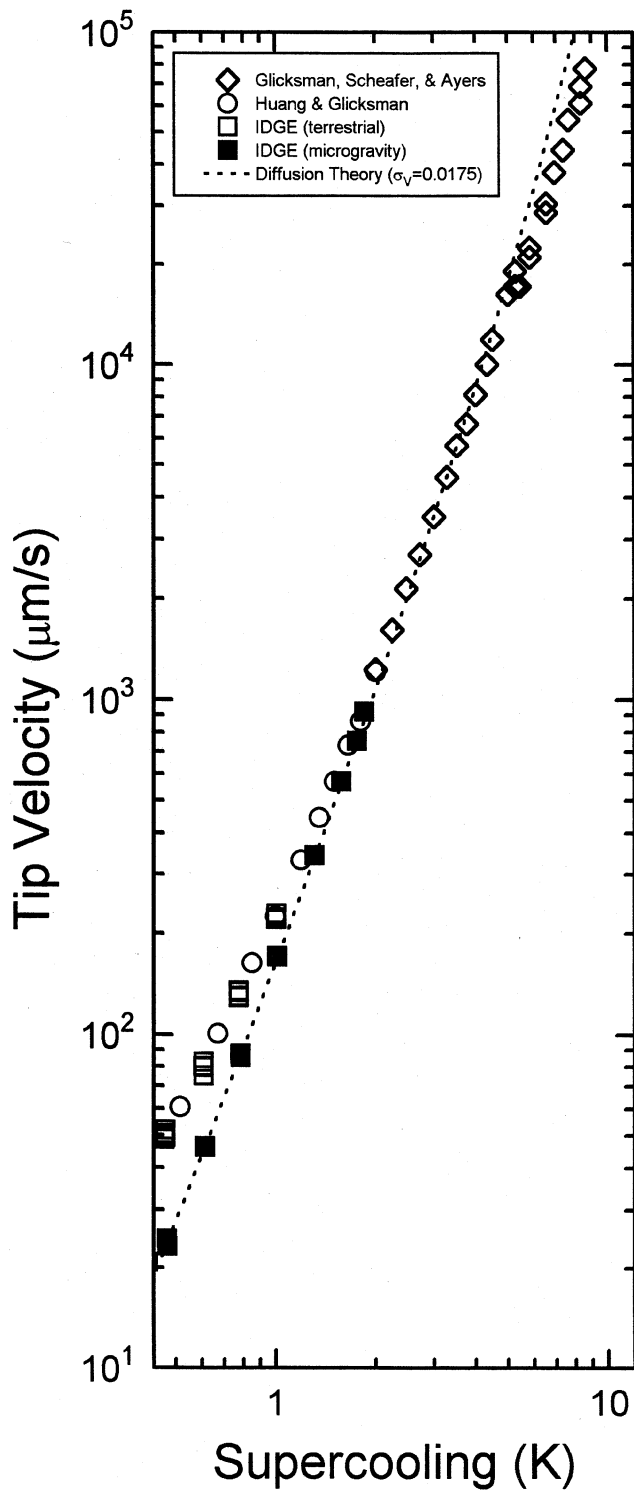


Fig. 7—Steady-state dendritic growth velocity vs supercooling at higher supercoolings. The theory line regressed to the microgravity data matches the data from Glicksman *et al.*'s experiments with succinonitrile up to a supercooling of approximately 5.0 K, where, perhaps, attachment kinetics become important.

dendrite approaches the nearest chamber wall; or (3) growth-to-growth variations in the side-branch pattern. We exhaustively analyzed this enhanced velocity scatter to investigate the effects of residual convection on dendritic growth, but the

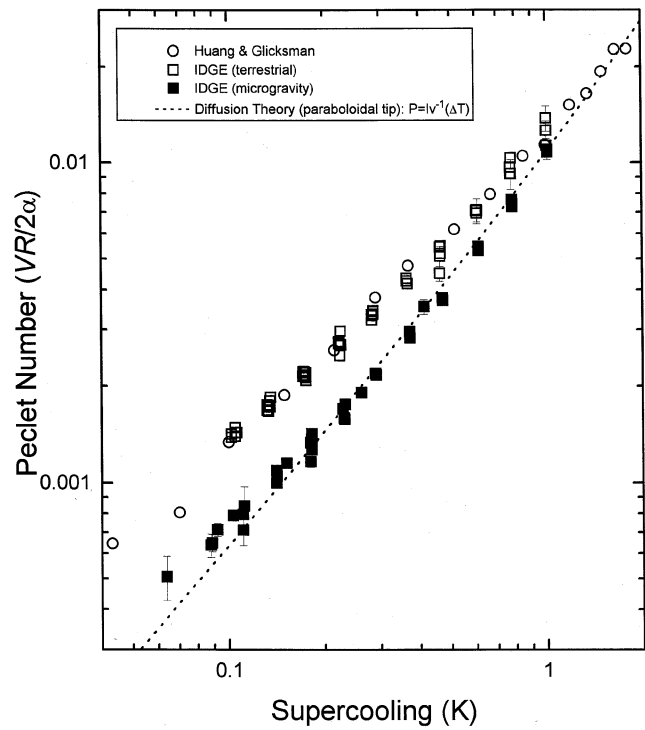


Fig. 8—Peclet number vs supercooling. The Peclet number is a zero parameter test of the Ivantsov model, as there are no adjustable parameters. The data are in approximate agreement with theory, except at the lower supercoolings where convective or chamber effects become important.

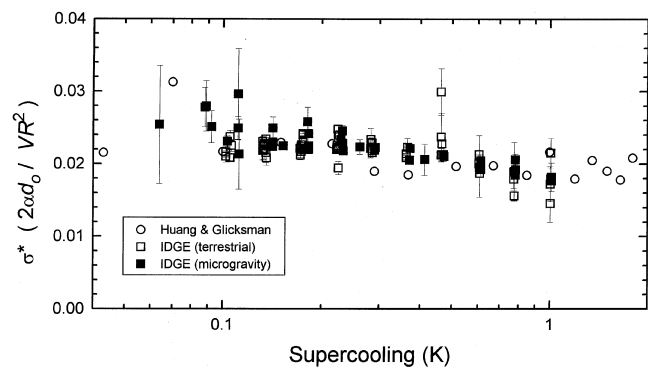


Fig. 9—The scaling rule vs supercooling. The scaling parameter data from both microgravity and terrestrial experiments are indistinguishable from each other. In spite of the large uncertainties in some of the measurements, the scaling parameter does not appear to be a constant over the full supercooling range of these experiments.

results remain inconclusive.^[32] Preliminary data and analysis obtained from a subsequent space flight experiment (February/March 1996) indicate that these large variations are not due to microgravity-driven convection.^[34] Although the overall lifting of the data from the predicted curve is most likely due to the wall proximity, the scatter in the data is not.^[35] It appears at this time, based on some current work derived from Schaefer^[36] on point-source calculations and thermal communication distances during dendritic growth, that this large scatter in velocity may be related to variations in the side-branching pattern.^[37,38]

B. Radii Data

Discussion of the tip radii measurements (Figure 6) parallels that given previously for the growth velocity data. Specifically, the two terrestrial data sets mutually agree, whereas the microgravity radii measurements remain slightly larger than the terrestrial measurements even at the highest supercoolings. At lower supercoolings, large differences develop between the microgravity radii data and the terrestrial data. The tip radius exhibits a weaker dependence on the supercooling compared to the velocity, so that the difference between the terrestrial and microgravity results is smaller, although also well resolved in these experiments. Again, at the lower supercoolings one observes (Figure 6) that the slope of the microgravity radii of curvature data appears to be parallel to that for the terrestrial tip radii data.

A self-consistent radius scaling constant, σ_R , was obtained by least-squares fitting the radii data, where the value for σ_R was calculated from the scaling expression for σ^* in Eq. [4] as follows:

$$\sigma_R = \frac{d_0}{I_v^{-1}(\Delta)R_{meas}} \quad [9]$$

A one-parameter fit to the radii data was calculated as the average of σ_R 's over the supercooling range 0.47 to 1.01 K. This procedure yields an average radii scaling parameter of $\sigma_R = 0.0185 \pm 0.0002$. This value of σ_R describes the microgravity radii data accurately only at the upper range of the IDGE supercoolings, again corroborating what appears to be the diffusion-limited and unconstrained range in this microgravity experiment. The difference between the self-consistent scaling constants σ_R and σ_V , calculated independently from the radii of curvature and from the growth velocity data, respectively, is over three times that of their combined uncertainties. This provides firm experimental evidence that the Ivantsov diffusion theory combined with a unique selection or scaling constant σ^* will not consistently predict dendritic growth characteristics even over a limited range of supercoolings.

Growth velocities and tip radii were the physical quantities characterizing dendritic crystal growth that we measured, so it is important to examine them thoroughly and to compare the terrestrial and microgravity results. The theory that has been under consideration, however, relies on a combination of the Ivantsov diffusion solution and interface selection or scaling physics. One or both of these components are inconsistent with our data.

C. Peclet Number Data

A test of the diffusion component of the theory only may be performed by examining the Peclet number data (Figure 8). Again, note that the two terrestrial data sets for the Peclet number agree. This is expected insofar as the individual velocity and tip radii data that were combined to form the Peclet number data were already shown to be in agreement. The Peclet numbers obtained under microgravity conditions are also shown to be strikingly different from the terrestrial data, as expected, and much closer to the predictions from theory. This constitutes a zero-parameter test. Close inspection of these data reveals small but significant differences between theory and experiment. Specifically, the Peclet number measurements at lower supercooling are generally larger

than those predicted from theory, whereas at higher supercoolings, the observed results are smaller.

The velocity and radii analyses described previously indicate that for the growth conditions attending the IDGE (both in terms of chamber size and acceleration levels), the supercooling range above 0.47 K results in *diffusion-limited* and *unconstrained* dendritic growth. If the detail of the Peclet numbers over this restricted supercooling region is enhanced (Figure 10), one sees that the microgravity Peclet numbers are systematically lower than those predicted by the Ivantsov solution. A least-squares analysis, weighted by the estimated uncertainties of the measurements, indicates that there is an insignificant probability that the Ivantsov solution, as expressed by Eq. 2, could produce the sum-squared differences observed between the theory and these data. Treating the thermal diffusivity, α , as the single "adjustable" parameter in the Ivantsov formulation, and performing a least-squares fit of the theoretical expression to these data, reduces α by 5 pct from the best value in the literature (the estimated total uncertainty of which is 3 pct). However, even with this one adjustable parameter, only a small probability exists for sum-squared differences between and the theory and the data being as large as we obtained.

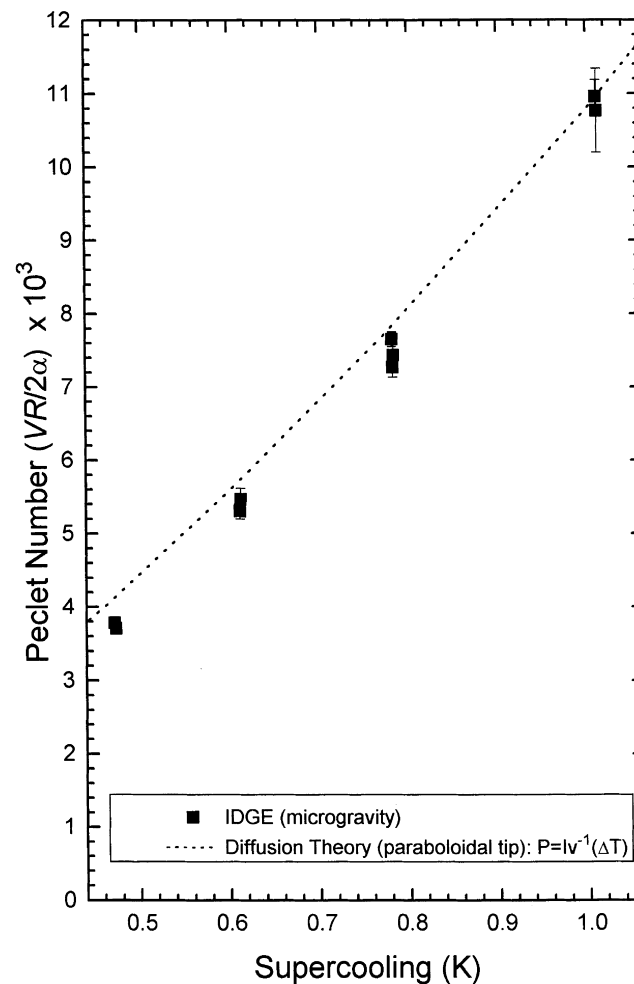


Fig. 10—Detailed view of the Peclet number vs supercooling in the supercooling range where dendritic growth is diffusion limited with the boundary conditions at infinity. Although the theory matches the data at 1.0 K supercooling, the rest of the data in this range is significantly below that calculated by theory.

Without treating α as an adjustable parameter, the experimental Peclet numbers are lower than the theoretical predictions; or alternatively, it takes less than the applied supercooling to obtain the corresponding theoretical Peclet number from Eq. 1. Several phenomenological adjustments reducing the supercooling are possible within the theory as follows: (1) a kinetic term proportional to V ; (2) a capillary term proportional to R^{-1} ; (3) a uniform supercooling reduction δT ; and (4) a fixed percentage reduction of the supercooling ΔT . All such modifications yielded calculated Peclet numbers such that the sum-squared differences between the phenomenological theory and the measured Peclet numbers were too large to be probable. Pines *et al.*^[39] have compared our data to a model of McFadden and Coriell^[40] that includes the density change on solidification (Stefan wind) and show an improved agreement between model and data. However, in our opinion, this improvement is similar to our phenomenological modeling; *i.e.*, the sum-squared differences is reduced, but not enough to conclude that data and model agree.

D. Selection Constant

Prior to the availability of this dendritic growth data set measured under diffusion-limited conditions in microgravity, it was not possible to test separately the Ivantsov solution and the interfacial selection hypothesis. The microgravity data provide the first firm evidence that shows how close the Ivantsov formulation for paraboloidal dendritic growth describes diffusion-limited, unconstrained dendritic growth in SCN. The approximate agreement reported here between predictions based on transport theory and the microgravity data suggests that dendritic growth in pure SCN is indeed governed by the diffusion of latent heat from the crystal–melt interface, but the standard Ivantsov formulation describing that diffusion process for a paraboloidal crystal is, nevertheless, in need of some modification.

The microgravity space flight results reported here help assess some aspects of interfacial selection or scaling theory. Specifically, a selection constant σ^* was calculated from Eq. 4, using measurements of V and R , and it was shown that $\sigma^* = 0.0196 \pm 0.0004$. This value pertains to data observed over the supercooling range above 0.47 K, where convection effects, side-branching effects, and chamber size limitations appear minimal, but below 1.0 K, where the most accurate radii measurements can be obtained. It is interesting that this value of σ^* is the same as that found in prior terrestrial experiments,^[15] *viz.*, $\sigma^* = 0.0195 \pm 0.0005$, and from the IDGE instrument when operated terrestrially, *viz.*, $\sigma^* = 0.0208 \pm 0.0006$. However, these values of the selection constant are significantly different from the individual adjustable scaling parameters used to fit the velocity data ($\sigma_V = 0.0175 \pm 0.0001$) or the radii data ($\sigma_R = 0.0185 \pm 0.0002$). There does not appear to be a *single* scaling constant, that, when coupled to Ivantsov's diffusion equation, properly describes *both* the growth velocity and tip radii data. The lack of a unique σ^* value may be attributed to the failure of Ivantsov's transport solution to predict accurately the Peclet number for diffusion-limited unconstrained dendritic growth.

The selection/scaling rule itself warrants more detailed scrutiny. Specifically, the scatter both within and among the three independently measured σ^* data sets is significant.

Large scatter makes a highly detailed analysis difficult, and somewhat speculative, but it appears that σ^* decreases slightly with the applied supercooling. This conclusion is borne out in several ways. First, if one were to extend the supercooling range over which the average value of σ^* was calculated, one obtains $\sigma^* = 0.0216 \pm 0.0011$ for Huang and Glicksman, $\sigma^* = 0.0217 \pm 0.0003$ for the IDGE operated terrestrially, and $\sigma^* = 0.0226 \pm 0.0005$ for the IDGE in microgravity. Although the three independently measured σ^* 's agree within statistical limits over the entire supercooling ranges investigated, the individual σ^* values differ from those calculated from the restricted supercooling range. Thus, σ^* does not appear to be strictly constant over the full range of supercoolings investigated.

To assess the possible dependence of σ^* on supercooling, we performed a least-squares regression, applied over the full range of supercooling, to the following power-law equation:

$$\sigma^*(\Delta T) = \sigma_0 \Delta T^n \quad [10]$$

where n and σ_0 are fitted parameters. If σ^* were independent of supercooling, then the fitted values of n would, within experimental uncertainty, be close to zero. Additionally, σ_0 would be close to the average of the measured σ^* values calculated previously. For the three σ^* data sets under consideration, we find exponents $n = 0.085 \pm 0.038$ for Huang and Glicksman, $n = -0.088 \pm 0.017$ for IDGE terrestrial, and $n = -0.131 \pm 0.014$ for IDGE microgravity. In the case of the IDGE terrestrial and microgravity data, the exponent of ΔT appears to be nonzero, including the estimated uncertainties. Moreover, examining in detail the nine σ^* data points calculated in the IDGE unconstrained diffusion-limited range, one obtains an average value of $\sigma^* = 0.0196$, which inadequately describes the behavior of these data over that supercooling range (Figure 11). A regression to the power law given by Eq. 10 for the σ^* data over the diffusion-limited range yields a power-law exponent $n = -0.203 \pm 0.045$ that is larger, or more supercooling dependent, than the exponent obtained using the full IDGE supercooling range. This analysis could be performed for functional forms of σ^* other than power law in Eq. 10, but the conclusions would remain the same; *i.e.*, σ^* appears to be slightly dependent on supercooling.

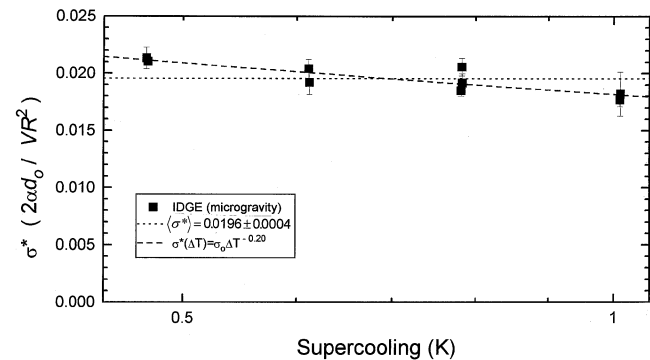


Fig. 11—Detailed view of the scaling parameter *vs* supercooling in the supercooling range where dendritic growth is diffusion limited with the boundary conditions at infinity. Even in this reduced supercooling range, the scaling parameter cannot be described by a single average value. The temperature dependence of the scaling parameter in this supercooling range is greater than over the full supercooling range.

Finally, despite the slight dependence of σ^* on supercooling, and the observation that the terrestrial and microgravity growth velocity and radii data differ markedly at every supercooling, the σ^* measurements from the two independent terrestrial data sets are almost statistically indistinguishable from those measured in the microgravity environment at the same applied supercooling (Figure 9). This suggests that convective effects do not play a measurable role in the value of σ^* for these experiments. However, multiple growths at one supercooling performed on a second microgravity space flight indicate that there may be a small statistical difference^[41]

V. SUMMARY AND CONCLUSIONS

Dendritic growth velocities and tip radii for pure SCN were measured under both microgravity and terrestrial gravity conditions. The in-orbit microgravity data, when compared to terrestrial dendritic growth data obtained using the same apparatus and techniques, demonstrate the following. (1) Convective effects under terrestrial conditions cause growth-speed increases up to a factor of 2 at the lower supercoolings ($\Delta T < 0.5$ K), and these effects remain discernible under terrestrial conditions up to supercoolings as high as 1.7 K. (2) In the supercooling range above 0.47 K, microgravity data remain virtually free of convective, neighboring dendrites, or chamber/wall proximity effects, and may be used reliably for critical examination of diffusion-limited unconstrained dendritic growth theories. (3) The Ivantsov diffusion solution, combined with a unique scaling constant σ^* , fails to yield consistent predictions for both the growth velocity and dendritic tip radii. (4) Peclet numbers predicted by Ivantsov's solution, although much closer to the microgravity data than the terrestrial data, deviate systematically (up to about 15 pct) from the microgravity data observed under diffusion-limited and unconstrained conditions. Preliminary data obtained from a second microgravity space flight experiment in March 1996 confirms this.^[41] (5) The selection parameter σ^* appears to be a slightly dependent on the supercooling. Lastly, (6), the σ^* measurements obtained from terrestrial and microgravity data are in good agreement with each other, despite a difference of over six orders of magnitude in the quasi-static acceleration. Again, the authors stress that any conclusion drawn about σ^* must remain somewhat tentative. The preliminary data obtained from the second flight experiment only partially confirm conclusions (5) and (6) at this time. Measurements and analysis to further engage these issues are currently in progress, and will be reported at a later date, as will data from a different material system (pivalic acid).

The most important aspect of these results is the comparison of the experimental Peclet numbers to the predictions from Ivantsov's model. For a simple model with minimal but important assumptions, the overall agreement between transport theory and experimental results is good. This validates the role of thermal conduction in ordinary dendritic growth and suggests that in the first order, an SCN dendrite is closely described by a paraboloid of revolution. Thus, Ivantsov's solution continues to play a key role in modeling of early solidification microstructures. This finding is especially noteworthy because the measurements reported here show validity for a model that remains useful today, but that

was proposed over 50 years ago. This validation took a half-century, awaiting the advent of microgravity experiments. At the same time, the results expose a systematic lack of agreement between theory and experiment that is clearly beyond the estimated uncertainties. This finding demands a search for and incorporation of solidification mechanisms that will bring theory or models closer to experimental results. Candidates for modification to the Ivantsov formulation are abundant. Now, as never before, detailed computations can demonstrate the proper way to include the effects of side branching, neighboring dendrites, kinetics, shape anisotropy, or other dendritic attributes. The authors offer here one key and well-recognized observation: the diffusion field of the Ivantsov formulation is based on a *steady-state* dendrite that is a *paraboloid* of revolution. This experiment, and measurements and calculations by others, show that these are heuristic assumptions,^{15,27,36,42} the implication of which require additional critical examination, both theoretical and experimental. The microgravity data reported here, especially those in the diffusion-limited regime, help constrain the allowable possibilities for further theoretical or numerical modeling. Indeed, the diffusion-limited growth data serve as a benchmark for testing and developing theories and provide a more firm empirical basis for phenomenological models of dendritic growth kinetics. The included tabulation here of the dendritic growth velocity and radius of curvature data from the first flight experiment will facilitate such future studies. We will proffer the data and descriptive reports from our 1996 and 1997 microgravity experiments as soon as it is practicable.

ACKNOWLEDGMENTS

The requirements for designing, building, testing, and operating a complex, highly interactive scientific microgravity experiment in low-earth orbit are beyond the skills and resources of any one individual or organization. An infrastructure, and diverse teams of dedicated professionals are required. Over the last 10 years, the following individuals contributed significantly to the design, construction, and operation of this experiment, which enabled the acquisition of the results contained herein. We thank R.C Hahn, B.A. Herbach, P.A. Kobryn, K.K. Koo, T.A. Lograsso, E.R. Rubinstein, N.B. Singh, M.E. Selleck, S.H. Tirmizi, and A. Velosa, all at Rensselaer Polytechnic Institute (Troy, NY). In addition, we thank R. Abramczyk, C. Blachly-Olah, D. Burns, A. Fedak, R. Grant, A. Kawecki, F. Kohl, G. Kraft, M. Lehto, L. Levinson, D. Malarik, J. McDade, D. Miller, A. Patel, D. Priebe, J. Robertson, A. Sobota, D. Vachon, G. Weeks, and R. Whittlesey, all at or associated with NASA's Glenn (formerly Lewis) Research Center (Cleveland, OH). Special thanks are also due for the continued understanding, interest, and financial support provided by the National Aeronautics and Space Administration, Life and Microgravity Sciences and Application Division (Code U, Washington, DC), under Contract No. NAS3-25368, with liaison provided by Microgravity Science Division (formerly the Space Experiments Division), NASA-Glenn Research Center. The successful operation of the experiment would not have been possible without the efforts of the USMP-2 Mission Scientist and the associated Mission Management team at the Marshall Space Flight Center. Thanks also goes to those who oversaw POCC training and simulations and the POCC cadre

Table III. Selected Thermophysical Properties of Succinonitrile*

Symbol	Property	Value	Remark	Ref.
κ_l	thermal conductivity at T_m	$5.32 \pm 0.15 \times 10^{-4}$ cal/cm s K	refers to unpublished research in Ref. 14	14
$c_{p,l}$	constant pressure specific heat	38.37 ± 0.1 pct cal/ mol K	at 335 ± 0.02 K	43
$c_{p,l}$	constant pressure specific heat	38.52 ± 0.1 pct cal/ mol K	at 340 ± 0.02 K	43
Δh_f	heat of fusion	885.1 cal/mol, assume ± 0.5 cal/mol	—	43
T_m	equilibrium melting temperature	331.233 ± 0.002 K	at SCN triple point	15
γ_{sl}	solid-liquid interfacial energy at T_m	8.94 ± 0.5 erg/cm ²	—	44
W	molecular weight	80.092 g/mol, without significant uncertainty	chemical formula and periodic table	—
ρ_s	density of solid at 25 °C	1.034 g/cm ³ , assume ± 0.005 g/cm ³	Finback quoted by Wulff and Westrum in Ref. 43	45
ρ_s	density of solid at 45 °C	1.023 g/cm ³ , assume ± 0.005 g/cm ³	Finback quoted by Wulff and Westrum in Ref. 43	45
(dT_m/dP)	change of T_m with pressure	0.0245 ± 0.005 K/atm	IDGE measurement	46
$c_{p,l}$	constant pressure specific heat at T_m	38.26 ± 0.06 cal/mol K	extrapolate from $c_{p,l}$ at 335 and 340 K	—
ρ_s	density of solid at T_m	1.016 ± 0.007 g/cm ³	extrapolated from ρ_s at 25 °C and 45 °C	—
Δv_{sl}	molar volume change on melting/freezing	2.70 ± 0.06 cm ³ /mol	calculated from Clapeyron equation, $(dT_m/dP) = T_m \Delta v_{sl} / \Delta h_f$	—
ρ_l	density of liquid at T_m	0.982 ± 0.007 g/cm ³	calculated from $\rho_l = (1/\rho_s + \Delta v_{sl}/W)^{-1}$	—
Ω_l	molar volume of liquid at T_m	81.6 ± 0.6 cm ³ /mol	calculated from $\Omega_l = W/\rho_l$	—
α_l	thermal diffusivity of liquid at T_m	1.134×10^5 $\mu\text{m}^2/\text{s} \pm$ 3 pct	calculated from $\alpha_l = \kappa_l/(c_{p,l}\rho_l)$	—
$\Delta h_f/c_{p,l}$	unit supercooling	23.13 K ± 0.2 pct	calculated from $\Delta h_f/c_{p,l}$	—
d_0	capillarity length	2.821×10^{-3} $\mu\text{m} \pm$ 6 pct	calculated from Eq. [3]	—

*In this table, *s* and *l* refer to the solid and liquid bcc phases. In the body of the article, all thermophysical properties refer to the liquid phase unless otherwise noted.

who coordinated and implemented the project's space flight operations. Finally, we also extend our deepest thanks to the crew of STS-62 and the support groups at all the NASA research centers involved with the space shuttle's activities.

APPENDIX I. Thermophysical properties

In the course of conducting and reporting on the work that culminates in this article, the authors discovered that some of the differences reported among the results of different experiments or different researchers are linked directly to differences in the values of the thermophysical properties used in the data analysis. To minimize this issue in the analysis reported in this article, we conducted a thorough literature review to ascertain accurate published measurements, and established uncertainties, for the values of the required properties (Table III). In the course of this review, we found some typographical mistakes, round-off errors, and noted that many of the listed values in the literature were not primary measurements, but were calculated or extrapolated from other measured primary values. They represent, consequently, secondary or derived values. In the preparation of this article, the authors have taken the most accurate measurements, and their associated uncertainties (which were estimated when not available), and calculated all derived values. In one case, we used our own primary

measurement.^[46] The values of the thermophysical properties used in this article are summarized in Table III. In Table III, α_l , $\Delta h_f/c_{p,l}$, and d_0 are required for the analysis; $c_{p,l}$, ρ_s , Δv_{sl} , ρ_l , and Ω_l are secondary or derived values; and κ_l , $c_{p,l}$, Δh_f , T_m , γ_{sl} , W , ρ_s , and (dT_m/dP) are the primary published or measured values of the thermophysical properties used to calculate the values of the thermophysical properties needed in the analysis.

REFERENCES

1. G.P. Ivantsov: *Dokl. Akad. Nauk, USSR*, 1947, vol. 58, p. 56.
2. M.E. Glicksman and S.P. Marsh: in *The Dendrite, Handbook of Crystal Growth*, D.J.T. Hurle, ed., Elsevier Science Publishers B.V., Amsterdam, 1993, vol 1b, p. 1077.
3. G.B. McFadden, A.A. Wheeler, R.J. Braun, S.R. Coriell, and R.F. Sekerka: *Phys. Rev. E*, 1993, vol. 48, p. 2016.
4. A. Karma and W.-J. Rappel: *Phys. Rev. Lett.*, 1996, vol. 77, p. 4050.
5. M.J. Bennett and R.A. Brown: *Phys. Rev. B*, 1989, vol. 39, p. 11705.
6. V. Pines, M. Zlatkowsky, and A. Chait: *Phys. Rev. A*, 1990, vol. 42, p. 6137.
7. M.D. Kunka, M.R. Foster, and S. Tanveer: *Phys. Rev. E*, 1997, vol. 56, p. 3068.
8. A. Papapetrou: *Z. fur Kristallographie*, 1935, vol. 92, p. 89.
9. J.S. Langer: *Rev. Mod. Phys.*, 1980, vol. 52, p. 1.
10. P. Pelce: *Dynamics of Curved Fronts*, Academic Press, New York, NY, 1988.
11. J.S. Langer and H. Muller-Krumbhaar: *Acta Metall.*, 1978, vol. 26, pp. 1681, 1689, and 1697.
12. J.S. Langer: *Science*, 1989, vol. 243, p. 1150.

13. E.A. Brener and V.I. Mel'nikov: *Adv. Phys.*, 1991, vol. 40, p. 53.
14. M.E. Glicksman, R.J. Schaefer, and J.D. Ayers: *Metall. Trans. A*, 1976, vol. 7A, pp. 1747-59.
15. S.C. Huang and M.E. Glicksman: *Acta Metall.*, 1981, vol. 29, pp. 701 and 717.
16. M.E. Glicksman and S.C. Huang: in *Convective Heat Transfer during Dendritic Growth, Convective Transport and Instability Phenomena*, J. Zierep and H. Ortel, eds., G. Braun, Karlsruhe, Germany, 1982, p. 557.
17. D.A. Saville and J. Beaghton: *Phys. Rev. A*, 1988, vol. 37, p. 3423.
18. R. Ananth and W.N. Gill: *J. Cryst. Growth*, 1988, vol. 91, p. 587.
19. R. Ananth and W.N. Gill: *J. Cryst. Growth*, 1991, vol. 108, p. 173.
20. R.F. Sekerka, S.R. Coriell, and G.B. McFadden: *J. Cryst. Growth*, 1995, vol. 154, p. 370.
21. M.E. Glicksman, E.A. Winsa, R.C. Hahn, T.A. LoGrasso, S.H. Tirmizi, and M.E. Selleck: *Metall. Trans. A*, 1988, vol. 19A, pp. 1945-53.
22. J.R. Schrieffer: *Review of Microgravity Science and Applications Flight Programs*, University Space Research Association, Washington, DC, 1987.
23. M.E. Glicksman, M.B. Koss, and E.A. Winsa: *JOM*, 1995, vol. 47 (8), p. 49.
24. M.E. Glicksman, M.B. Koss, and E.A. Winsa: *Phys. Rev. Lett.*, 1994, vol. 73, p. 573.
25. M.E. Glicksman, R.C. Hahn, M.B. Koss, S.H. Tirmizi, A. Velosa, and E.A. Winsa: *Adv. Space Res.*, 1991, vol. 11, p. 53.
26. E.R. Rubinstein, S.H. Tirmizi, and M.E. Glicksman: *J. Cryst. Growth*, 1990, vol. 106, p. 89.
27. M.E. Glicksman, M.B. Koss, V.E. Fradkov, M.E. Rettenmayr, and S.S. Mani: *J. Cryst. Growth*, 1994, vol. 137, p. 1.
28. J.C. LaCombe, M.B. Koss, V.E. Fradkov, and M.E. Glicksman: *Phys. Rev. E*, 1995, vol. 52, p. 2278.
29. M.B. Koss, M.E. Glicksman, L.T. Bushnell, J.C. LaCombe, and E.A. Winsa: *8th Int. Symp. on Experimental Methods for Microgravity Materials Science*, R.A. Schiffman, ed., TMS, Warrendale, PA, 1995, p. 51.
30. M.E. Glicksman, M.B. Koss, L.T. Bushnell, J.C. LaCombe, and E.A. Winsa: *Iron Steel Inst. Jpn.*, 1995, vol. 35, p. 604.
31. M.E. Glicksman, M.B. Koss, L.T. Bushnell, J.C. LaCombe, and E.A. Winsa: *Materials Research Society Symposia Proceedings*, F. Family, P. Meakin, B. Sapoval, and R. Wool, eds., Materials Research Society, Pittsburgh, PA, 1995, vol. 367, p. 13.
32. M.B. Koss, L.T. Bushnell, M.E. Glicksman, and J.C. LaCombe: *Chem. Eng. Comm.*, 1996, vols. 152-153, p. 351.
33. V. Pines, A. Chait, and M. Zlatkowski: *J. Cryst. Growth*, 1996, vol. 167, p. 383.
34. L.A. Tennenhouse, M.B. Koss, J.C. LaCombe, and M.E. Glicksman: *J. Cryst. Growth*, 1997, vol. 174, p. 82.
35. L.A. Tennenhouse, M.B. Koss, J.C. LaCombe, A.O. Lupulescu, and M.E. Glicksman: Rensselaer Polytechnic Institute, Troy, NY, unpublished research, 1998.
36. R.J. Schaefer: *J. Cryst. Growth*, 1978, vol. 43, p. 17.
37. J.C. LaCombe, M.B. Koss, D.C. Corrigan, L.A. Tennenhouse, A.O. Lupulescu, and M.E. Glicksman: *J. Cryst. Growth*, 1999, in press.
38. D.C. Corrigan, M.B. Koss, K.D. deJager, L.A. Tennenhouse, J.C. LaCombe, and M.E. Glicksman: *Phys. Rev. E*, 1999, in press.
39. V. Pines, A. Chait, and M. Zlatkowski: *J. Cryst. Growth*, 1996, vol. 169, p. 798.
40. G. McFadden and S. Coriell: *J. Cryst. Growth*, 1986, vol. 74, p. 507.
41. A.O. Lupulescu, M.B. Koss, J.C. LaCombe, M.E. Glicksman, and L.A. Tennenhouse: Rensselaer Polytechnic Institute, Troy, NY, unpublished research, 1998.
42. A. Dougherty, P.D. Kaplan, and J.P. Gollub: *Phys. Rev. Lett.*, 1987, vol. 58, p. 1652.
43. C.A. Wulff and E.F. Westrum: *J. Phys. Chem.*, 1963, vol. 67, p. 2376.
44. R.J. Schaefer, M.E. Glicksman, and J.D. Ayers: *Phil. Mag.*, 1975, vol. 32, p. 725.
45. Finback: *Arch. Math. Naturvidenskab*, 1938, vol. B42-1, p. 71; *Chem Abstr.*, 1940, vol. 34, p. 12.
46. J.C. LaCombe, M.B. Koss, L.A. Tennenhouse, E.A. Winsa, and M.E. Glicksman: *J. Cryst. Growth*, 1998, vol. 194, p. 143.